Developmental Cell, Vol. 9, 805–817, December, 2005, Copyright ©2005 by Elsevier Inc. DOI 10.1016/j.devcel.2005.10.016

Hexagonal Packing of *Drosophila* Wing Epithelial Cells by the Planar Cell Polarity Pathway

Anne-Kathrin Classen,[1] Kurt I. Anderson,[1,2] Eric Marois,[1] and Suzanne Eaton[1,*]
[1] Max Planck Institute of Molecular Cell Biology and Genetics
Pfotenhauerstrasse 108
01309 Dresden
Germany

Summary

The mechanisms that order cellular packing geometry are critical for the functioning of many tissues, but they are poorly understood. Here, we investigate this problem in the developing wing of *Drosophila*. The surface of the wing is decorated by hexagonally packed hairs that are uniformly oriented by the planar cell polarity pathway. They are constructed by a hexagonal array of wing epithelial cells. Wing epithelial cells are irregularly arranged throughout most of development, but they become hexagonally packed shortly before hair formation. During the process, individual cell boundaries grow and shrink, resulting in local neighbor exchanges, and Cadherin is actively endocytosed and recycled through Rab11 endosomes. Hexagonal packing depends on the activity of the planar cell polarity proteins. We propose that these proteins polarize trafficking of Cadherin-containing exocyst vesicles during junction remodeling. This may be a common mechanism for the action of planar cell polarity proteins in diverse systems.

Introduction

The function of some epithelial tissues depends on the exact geometry of constituent cells. Sensory epithelia of the inner ear comprise an ordered array of hair cells and support cells (McKenzie et al., 2004; Tilney and Saunders, 1983; Tilney et al., 1986). To respond to mechanical perturbations caused by sound or motion, stereocilia bundles on sensory hair cells must be precisely aligned (Roberts et al., 1988).

The optical properties of vertebrate and invertebrate eyes depend on cellular packing geometry. In Dipteran eyes, which utilize neural superposition to increase their sensitivity, axons of rhabdomeres in different omatidia responding to the same spatial information converge to the same place in the lamina, superimposing their signals (Nilsson, 1989). Small deviations in packing within or between omatidia would make this system unworkable. In the vertebrate eye, hexagonal packing of lens fiber cells minimizes light scattering by cell membranes and is essential for transparency (Tardieu, 1988). How do cells form such precise geometrical arrays?

*Correspondence: eaton@mpi-cbg.de
[2] Present address: Beatson Institute for Cancer Research, Garscube Estate, Switchback Road, Glasgow G61 1BD, United Kingdom.

The developing wing of *Drosophila* provides an attractive genetic and cell biological system in which to address these questions. The wing is covered by a hexagonally packed array of hairs, each constructed by a single wing epithelial cell. Hairs are oriented distally and parallel to the longitudinal wing veins, and they have been proposed to guide air flow over the surface of the wing during flight (Wootton, 1992); regular hair spacing and orientation would clearly be important for this function. Genetic analysis has identified a group of "tissue polarity" or "planar cell polarity (PCP)" genes essential for global orientation of hairs on the wing surface (Gubb and Garcia-Bellido, 1982). These genes encode proteins that localize to adherens junctions and polarize to form tightly coupled proximal and distal cortical domains of different composition several hours before hair formation (Adler, 2002; Eaton, 2003; Strutt, 2002; Tree et al., 2002a). Here, we show that PCP proteins also have an essential role in generating orderly hexagonal packing of wing epithelial cells as they polarize along the proximal-distal axis.

Results

The Wing Epithelium Becomes Hexagonally Packed Shortly before Hair Formation

To study changes in epithelial packing, we developed an automated image analysis program (see Experimental Procedures). After staining developing wings for E-Cadherin, we used the program to identify each cell and to measure the length of each cell-cell contact, the total perimeter and area of each cell, and the number of its neighbors. We also identified three- and four-cell vertices in the epithelium. The analysis was performed at larval and prepupal stages, and at five pupal time points beginning at the P2B stage described by Waddington (Waddington, 1941) and ending at the time of hair outgrowth (Figure 1, see timeline in Table S1; see the Supplemental Data available with this article online).

Figures 1A–1G show processed images of wings at different developmental stages in which tetragonal, pentagonal, hexagonal, heptagonal, and octagonal cells are indicated by different colors. Intervein regions of three wings for each stage were quantified and averaged to generate the plots shown in Figures 1H–1J (a total of approximately 2500 cells per time point). Wing epithelial cells are irregularly packed throughout larval and prepupal development (Figures 1A and 1B). Less than half the cells are hexagonal, and of nonhexagonal cells, the majority are pentagons (Figure 1I); on average, each cell has less than six (5.55) neighbors.

The wing epithelium is repacked into a quasihexagonal array beginning shortly after the pupal molt and ending just before hair formation. Figures 1C–1G show regions surrounding longitudinal vein 3 (L3, see cartoon). Results for intervein cells are quantified in Figure 1I. Similar repacking occurs in other regions of the wing (Figures S1A–S1I; see Supplemental Data available with this article online). The increase in hexagons occurs mainly at the expense of pentagons, although

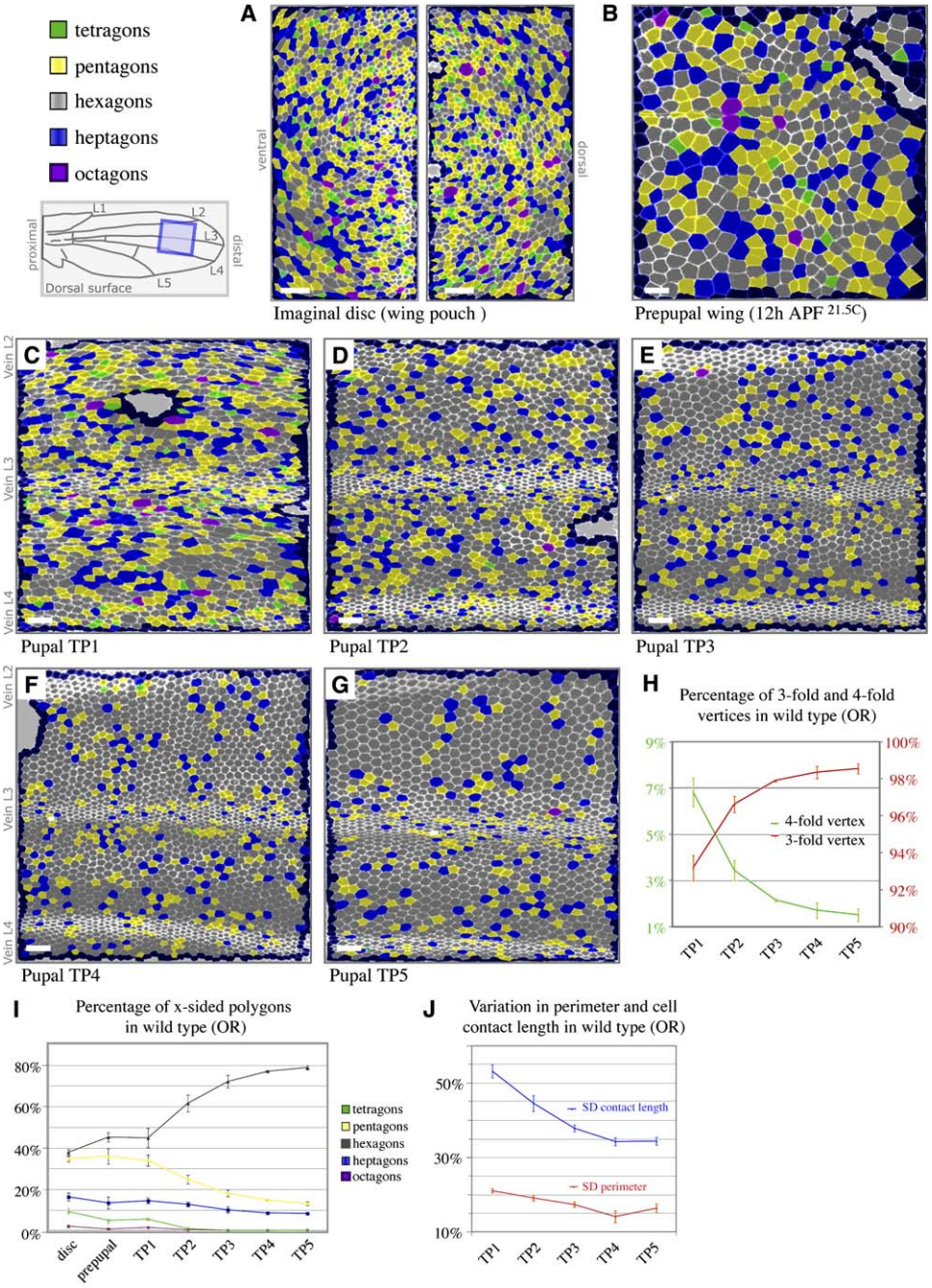

Figure 1. Changes in Packing of Wild-Type Wing Epithelia during Development

(A–G) The wing cartoons highlight the region of the wing. Epithelia become hexagonally packed during pupal development. Processed images of Cadherin-stained wings at (A) larval and (B) prepupal stages and at five different pupal times (TP1–TP5) from (C–G) Waddington stages P2B–P2C. The number of neighbors for each cell, determined by using Cellenger automated image analysis software, is color coded on the images. All scale bars are 10 μm.

(H) Percentage of 3-fold and 4-fold vertices during pupal stages TP1–TP5. Consistent with Euler's formula (F + V − E = 2), which describes the mathematical relationship between the total number of faces (F), vertices (V), and edges (E), the percentage of 3-fold vertices increases as the epithelium becomes more hexagonal.

(I) Percentage of cells with four, five, six, seven, or eight neighbors (color coded as indicated) at different developmental times.

(J) Variability in the total cell perimeter and individual cell edge length decreases between TP1 and TP4. Standard deviations are expressed as a percentage of the average perimeter (or average cell edge length) to control for cell size differences. Approximately 2500 cells per data point were averaged to obtain the data in (H)–(J). Only intervein cells on the dorsal side of the wing surface were analyzed.

smaller decreases in the number of four-, seven-, and eight-sided cells occur also (Figure 1I and Figures S1H and S1I). Consistent with Euler's formula, which defines the relationship between faces, edges, and vertices of polyhedra, the number of four-cell vertices decreases, and the number of three-cell vertices increases (Figure 1H) as the average neighbor number grows from 5.55 to 5.96. This means that there is a net increase in

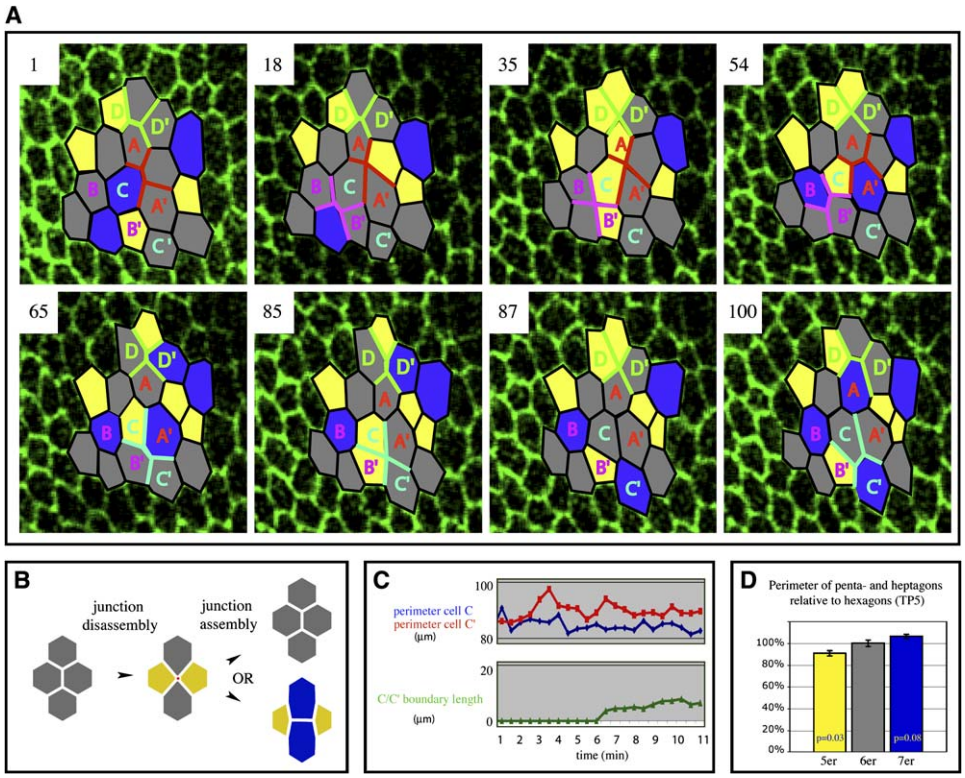

Figure 2. Junction Remodeling Occurs during Hexagonal Repacking

(A) Single images from a time-lapse series of stage-P2B pupal wings expressing Cadherin-GFP. Frame numbers (separated by 30 s) are indicated in the upper-left corner of each image. Overlaid on each frame is a color-coded cartoon of the region undergoing junction remodeling. Blue indicates heptagons, gray indicates hexagons, and yellow indicates pentagons. Cells and junctions that undergo remodeling are highlighted in different colors. The complete time lapse is available in Movie S1.

(B) Schematic illustration of junction remodeling events in pupal wings.

(C) Changes in the length of the perimeter of cells C and C′, and the growing boundary between them.

(D) Average perimeters of pentagonal, hexagonal, and heptagonal cells.

the number of cell contacts. Regularization of epithelial packing is also reflected in the decreased variability of the area (not shown) and perimeter (Figure 1J) of wing cells. Variation in individual junction lengths decreases even more than that of the cell perimeter (Figure 1J), consistent with junctional material becoming more symmetrically distributed between neighbors. Although the absolute number of cell contacts increases during hexagonal packing, the total perimeter is minimized, suggesting that total junctional material need not increase. By the time hairs form, intervein regions of the wing consist of 78% hexagons. These are arrayed in neat rows of coordinate orientation, occasionally interrupted by pentagons and heptagons. Similar regularization of cell packing occurs in the moth wing before scale formation (Nardi and Magee-Adams, 1986). These data show that generation of a hexagonally packed array of epithelial cells is a discrete developmental event, not a "ground state" of epithelia.

Intercellular Junctions Shrink and Grow during Hexagonal Repacking

To study how cell contacts were remodeled, we performed live confocal imaging on pupal wings expressing Cadherin:GFP (Oda and Tsukita, 2001) (Figure 2A, complete time-lapse in Supplemental Data). We often observed intercellular junctions shrinking to form a four-way vertex. Four-way vertices then resolved into a pair of three-way vertices (colored cell boundaries in Figure 2A, schematized in Figure 2B), sometimes by reexpanding the original cell boundary (green boundary between cells D and D′ in Figure 2A), or alternatively by assembling a junction between different cells in the perpendicular direction (red boundary between cells A and A′, turquoise boundary between cells C and C′, and pink boundary between cells B and B′). These events resemble those of embryonic convergent extension (Bertet et al., 2004; Oda and Tsukita, 1999; Zallen and Zallen, 2004); however they are not as strongly directional. This is consistent with the absence of dramatic concurrent changes in the proportions of the wing epithelium.

Assembly of new cell contacts takes place within 6–15 min—much more rapidly than junctions assemble de novo in embryonic epithelia (Tepass and Hartenstein, 1994). Thus, we wondered whether the junctional material that accumulates at these boundaries might derive from preexisting cell contacts rather than from the biosynthetic pathway. To approach this question, we asked whether growth of a new cell boundary added to the total cellular perimeter. Measuring the perimeter of cells C and C′ during the elongation of the boundary between them (Figure 2C) revealed that the length of the cell perimeter fluctuates over a period of several minutes. These fluctuations do not correlate with the development of the

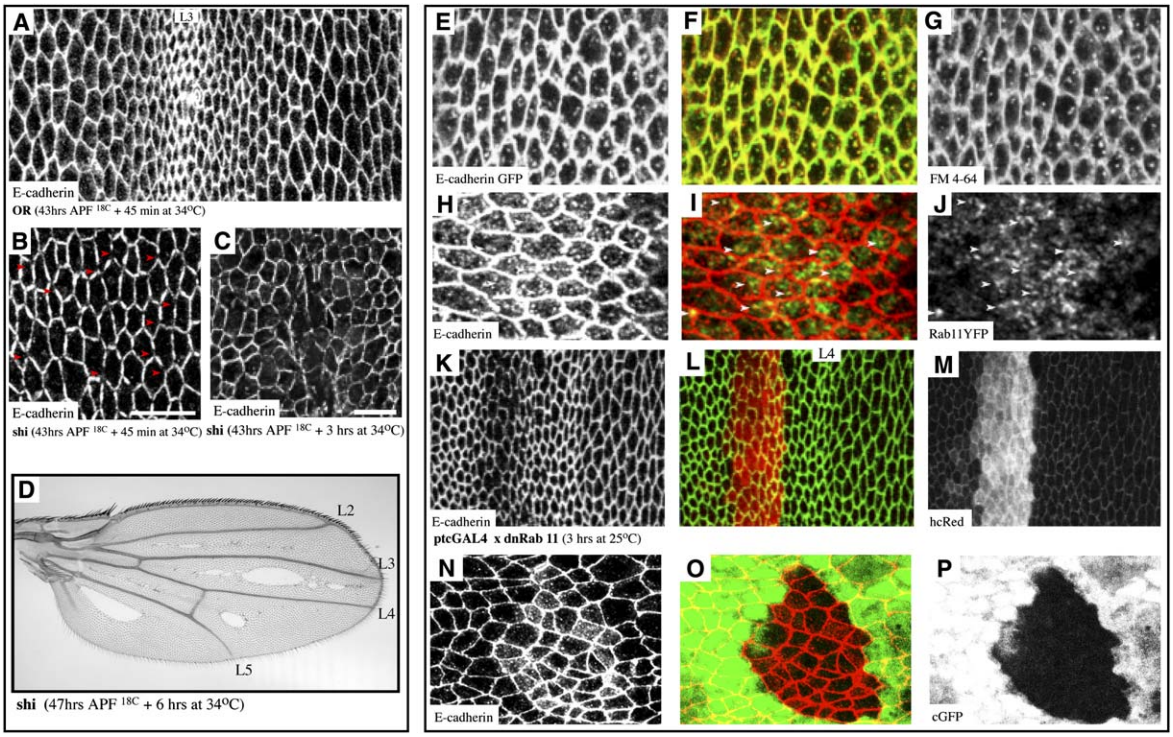

Figure 3. Cadherin Trafficking during Cortical Polarization

All scale bars are 10 μm.

(A–C) Projections of E-Cadherin-stained wings that include all sections with junctional E-Cadherin. (A) Intervein regions surrounding L3 of a wild-type wing stained for E-cadherin after a 45 min shift to 34ºC starting at stage P2B. The row of smaller cells stained more intensely for E-cadherin in the center of the image corresponds to L3. (B) *shi* pupal wing stained for E-cadherin after a 45 min shift to 34ºC starting in P2B. Red arrows indicate gaps in E-cadherin. (C) A *shi* wing (between L3 and L4) shifted for 3 hr to 34ºC starting in P2B.

(D) A *shi* adult wing shifted for 6 hr to 34ºC starting at P2B.

(E–G) A living pupal wing (stage P2B) that expresses (E and F) GFP-Cadherin (green) ubiquitously and has been stained with (F and G) FM4-64 (red) for 15 min. FM4-64 labels the plasma membrane and any endosomes that form after addition.

(H–J) A single apical optical section of a stage-P2B pupal wing ubiquitously expressing low levels of (I and J) YFP-Rab11 (green) stained for (H and I) E-Cadherin (red). Arrowheads indicate colocalization between Rab11 endosomes and E-Cadherin. Because this is not a projection of all optical sections with junctional Cadherin staining, the junctional staining appears discontinuous.

(K–M) A stage-P2B pupal wing that has expressed Rab11SN in the cells indicated in (M) for 3 hr. Rab11SN is expressed by using the pUhr vector (Marois et al., 2005) in which expression can be initiated after excision of an HcRed-containing FLP cassette between the UAS promoter and the cDNA. (K and L) E-Cadherin (green) begins to disappear from cell boundaries of Rab11SN-expressing cells (indicated by residual HcRed fluorescence in [L] and [M]).

(N–P) A $Sec5^{E13}$ clone marked by the absence of (O and P) GFP (green). (N and O) Cadherin (red) accumulates in internal vesicles in mutant tissue.

new cell boundary, however. Consistent with this, the average perimeter of five-, six-, and seven-sided cells did not differ by the length of a cell boundary, although we found small, but significant, differences between them (Figure 2D). These data suggest that the formation of new cell contacts may utilize material derived from contacts with other cells.

Dynamin Is Needed for Normal Cadherin Distribution during Junction Remodeling

How might Cadherin or other junctional material be added to a growing boundary? In other epithelia, Cadherin is dynamically endocytosed and recycled to modulate cell adhesion (Bryant and Stow, 2004). To test whether this might happen in the pupal wing, we used the temperature-sensitive *shibire* (*shi*) mutation of *dynamin*. Dynamin is required for scission of endocytic vesicles (Sever, 2002) and vesicles formed from Rab11 recycling endosomes (Pelissier et al., 2003; van Dam and Stoorvogel, 2002). A total of 30–45 min after shifting to 34ºC, gaps form in junctional E-Cadherin in *shi* mutant wings that are not found in wild-type control wings (compare Figures 3A and 3B), even after 3 hr of temperature shift (see Figure 4A). Similar results are obtained in clones of *shi* mutant cells (Figures S2F and S2G). The gaps form exclusively in intervein regions (not shown), and they occur primarily at or adjacent to vertices. Similar results were obtained for Armadillo, another adherens junction protein (not shown). In contrast, the septate junction protein Coracle (Figures S2I–S2L) and basolaterally localized CD2GFP (not shown) were undisturbed by loss of Dynamin. After 3 hr at 34ºC, *shi* mutant cells show even larger gaps in Cadherin (Figure 3C). By 6 hr, cell-free areas are seen in the intervein region by Cadherin staining (not shown). After these animals are restored to 18ºC, emerging adults have holes in wing intervein regions (Figure 3D). None of these changes are observed when temperature shifts are performed on third instar larvae (Figures S2A and S2B), even for longer times. Loss of Cadherin is not a consequence of cell

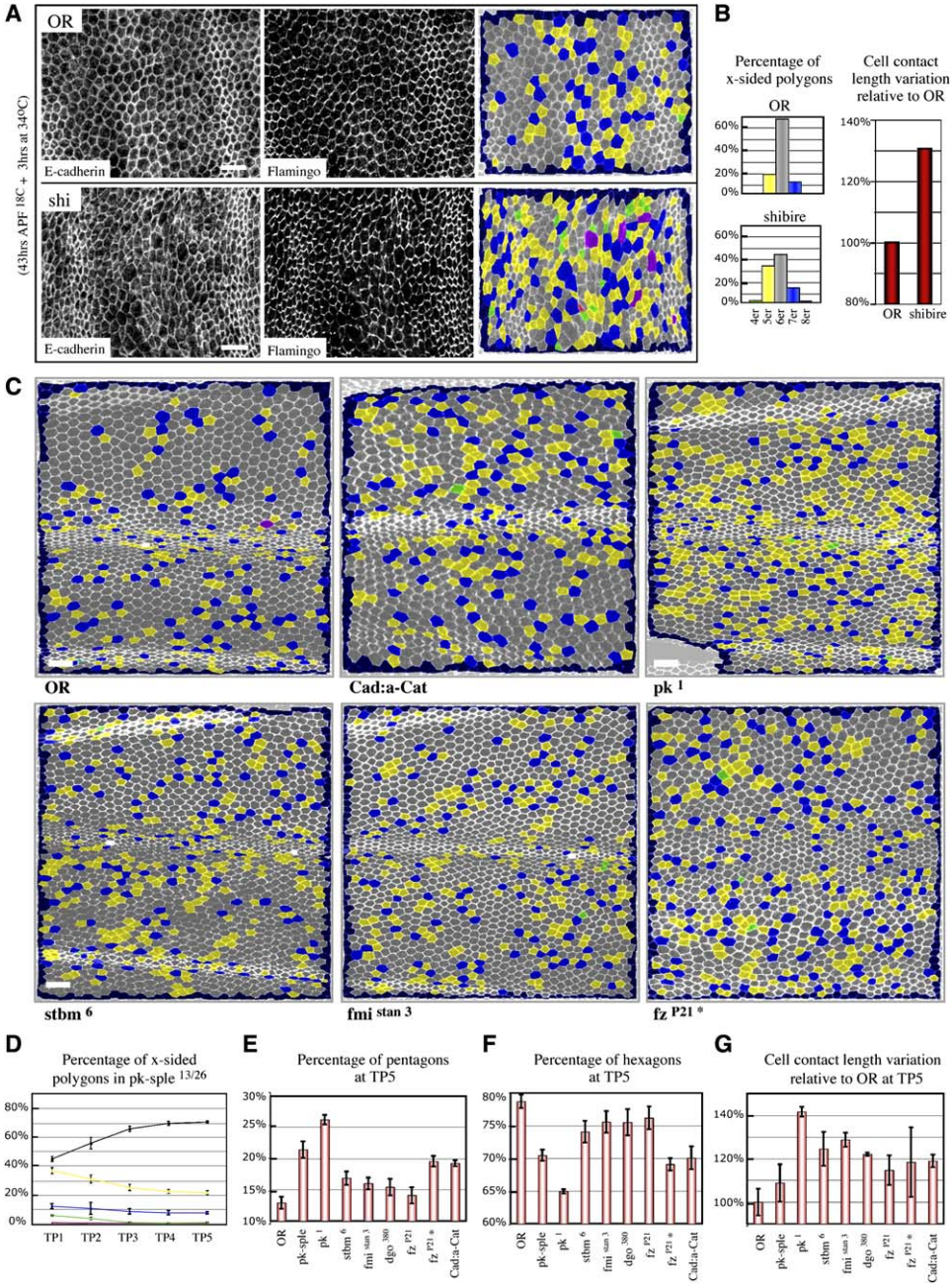

Figure 4. Defects in Hexagonal Packing Caused by PCP, Dynamin, and Cadherin Mutants

All scale bars are 10 μm.

(A) Upper panels: a wild-type wing shifted at P2B to 34ºC for 3 hr and stained for E-cadherin (left) and Fmi (middle). The right panel is color coded to show cell neighbor number. Lower panels: a *shi* mutant wing shifted at P2B to 34ºC for 3 hr and stained for E-cadherin (left panel) and Fmi (middle panel). Cell packing (right panel) is disturbed.

(B) Neighbor number and the variability of individual contact lengths of the wild-type and *shi* wings shown in (A).

(C) Neighbor number at TP5 (hair outgrowth) for wings of the indicated genotypes. Neighbor number is color coded as in Figure 1. For wings expressing Cad:a-Cat, cell boundaries were determined by Fmi staining, which becomes more uniform at hair outgrowth.

(D) Time course of cell packing of *pk-sple* from TP1 to TP5.

(E) Percentage of cells with five neighbors at TP5 in wild-type and mutant wings.

(F) Percentage of cells with six neighbors at TP5 in wild-type and mutant wings.

(G) Standard deviation of the length of individual cell boundaries is normalized to the standard deviation of the cell perimeters for three wings per genotype to correct for perimeter variability. For each mutant, this ratio is depicted as a percentage of the wild-type ratio. The average and standard deviation of the perimeters (in μm) of the different genotypes range from 16.8 ± 2.6 (for OregonR) to 15.1 ± 1.9 (for pk^1).

death; Cadherin is lost before Caspase is found in the nucleus (Figures S2C–S2E). These data suggest that Dynamin is required to maintain uniform localization of adherens junctions, but not septate junctions or basolateral proteins, during repacking. Development of holes in intervein regions where Cadherin gaps form suggests

that the loss of junctional proteins disturbs epithelial integrity.

To precisely define the stage at which Dynamin was required to maintain Cadherin, we systematically shifted *shi* mutants to 34ºC during a sliding 6 hr window starting just after pupariation and ending after hair formation. We quantified the frequency and placement of holes in the adult wing as a read-out because antibody penetration is prevented by the cuticle throughout much of pupal development. Although we observed a variety of phenotypes (summarized in Table S1), only temperature shifts initiated between P2A and mid-P2C (before hair formation) cause holes in the wing (Figure S2H). These data show that epithelial repacking is temporally coincident with the requirement for Dynamin.

To confirm that Cadherin enters the endocytic pathway at the time of hexagonal repacking, we stained GFP-Cadherin-expressing pupal wings (stage P2B) with FM4-64. FM4-64 labels the plasma membrane and endosomes that form after its addition. The majority of pupal wing cells contain multiple internal spots of GFP-Cadherin that colocalize with FM4-64 after 15–30 min (Figures 3E–3G). Thus, Cadherin is actively endocytosed during repacking.

To ask which type of endosomes contained Cadherin, we used flies that ubiquitously expressed YFPRab11 or CFPRab5 at low levels (Marois et al., 2005). Rab11 labels recycling endosomes, and Rab5 marks early endosomes (Zerial and McBride, 2001). Cadherin was observed in both types of endosomes (Figures 3H–3J and Figures S3H–S3J), supporting the idea that it is endocytosed and recycled.

In MDCK cells, Cadherin is delivered through Rab11 endosomes (Lock and Stow, 2005). To ask whether this occurs in the wing, we disturbed Rab11 function by short-term expression of the dominant-negative Rab11SN (Marois et al., 2005). A total of 3 hr after initiating Rab11SN expression, Cadherin begins to be lost from the junctional region—a phenotype similar to that of the *shi* mutant (Figures 3K–3M). These cells are not apoptotic (Figures S3A–S3D). No gaps form when Rab11SN is expressed for similar times in larval wing discs (Figures S3E–S3G). Thus, Rab11 is required to deliver Cadherin to junctions, and this requirement is acute during epithelial repacking. Loss of junctional E-Cadherin in *dynamin* mutant cells may reflect Dynamin's function at Rab11 endosomes.

The exocyst is a multiprotein complex that mediates polarized membrane delivery from recycling endosomes and from the golgi in many different cell types (Lipschutz and Mostov, 2002; Prigent et al., 2003; Sommer et al., 2005; Zhang et al., 2004). In the thorax, E-Cadherin delivery from recycling endosomes to the zonula adherens depends on exocyst components (Langevin et al., 2005). To test whether E-Cadherin was recycled via the exocyst during repacking in the wing, we utilized a mutation in Sec5 ($sec5^{E13}$) that has been suggested to preferentially perturb recycling (Sommer et al., 2005). Cadherin accumulates in internal vesicles and along the plasma membrane in $sec5^{E13}$ mutant cells (Figures 3N–3P). Accumulation of internal vesicles suggests that delivery of Cadherin is slowed. We do not know whether higher levels of peripheral Cadherin staining reflect accumulated unfused vesicles, or whether Sec5 may also function at some other step in Cadherin trafficking.

Hexagonal Packing Is Disturbed by Inhibiting Dynamin or Stabilizing E-Cadherin Contacts

To ask whether perturbing endocytosis and recycling caused defective cell packing, we analyzed *shi* mutant wings shortly after the shift to the restrictive temperature. Compared with wild-type shifted to the same temperature, *shi* tissue was less hexagonal and had a higher variability in the length of individual cell contacts (Figures 4A and 4B). This is consistent with the possibility that Dynamin-dependent recycling of junctional components is needed to remodel junctions; however, packing may have been perturbed by some other Dynamin-dependent process.

To test whether turnover of Cadherin itself was required for hexagonal packing, we induced expression of an E-Cadherin:α-Catenin fusion protein at the time of repacking (Dumstrei et al., 2002). A similar vertebrate construct is not regulated by β-catenin, causes abnormally stable adhesiveness, and inhibits motility in L cells (Nagafuchi et al., 1994). Expression of this construct disrupts hexagonal packing and increases the variability of cell contact lengths (Figures 4C and 4E–4G and Table S2). This is consistent with the idea that junction remodeling depends on the disassembly of E-Cadherin-mediated contacts, although we cannot rule out additional effects mediated by irreversible linkage to the actin cytoskeleton.

PCP Proteins Are Needed for Hexagonal Repacking

We suspected a link between the PCP pathway and epithelial repacking, because repacking occurs at the time that these proteins are thought to polarize. We therefore quantified neighbor number and junction length variability at the time of hair outgrowth in different PCP mutants (Figures 4C–4G and Table S2). For $pk\text{-}sple^{13/26}$, we also quantified neighbor number over time (Figure 4D).

$pk\text{-}sple^{13/26}$ wings begin repacking at the same time as wild-type (compare with Figure 1I); however, the process is less successful. Whereas wild-type wings reduce the percentage of pentagonal cells from 34% to 13% by the time that hairs begin to emerge, $pk\text{-}sple^{13/26}$ wings retain 21% (Figures 4D and 4E and Table S2). Thus, about 40% of the pentagonal cells that normally assemble boundaries with new neighbors (and become hexagonal) fail to do so in *pk-sple* mutants. Consistent with this, *pk-sple* wing epithelia contain abnormally high numbers of four-way vertices between cells (Figure S1G). pk^1 mutant wings are even more irregularly packed than $pk\text{-}sple^{13/26}$ wings (Figures 4C and 4E–4G and Table S2). A total of 62% of the pentagonal cells that would normally become hexagonal fail to assemble boundaries with new neighbors in pk^1 wings. Even four-sided cells accumulate significantly in pk^1 mutant wings (Table S2). Individual cell contact lengths are also much more variable; while $pk\text{-}sple^{13/26}$ boundary lengths were 9% more variable than wild-type, those of pk^1 were 42% more variable (Figure 4G and Table S2). These data are consistent with the earlier observation that adult *pk* wings frequently contain pentagonal cells (Gubb et al., 1999). They suggest that the assembly of new cell boundaries and regularization of junction length do not

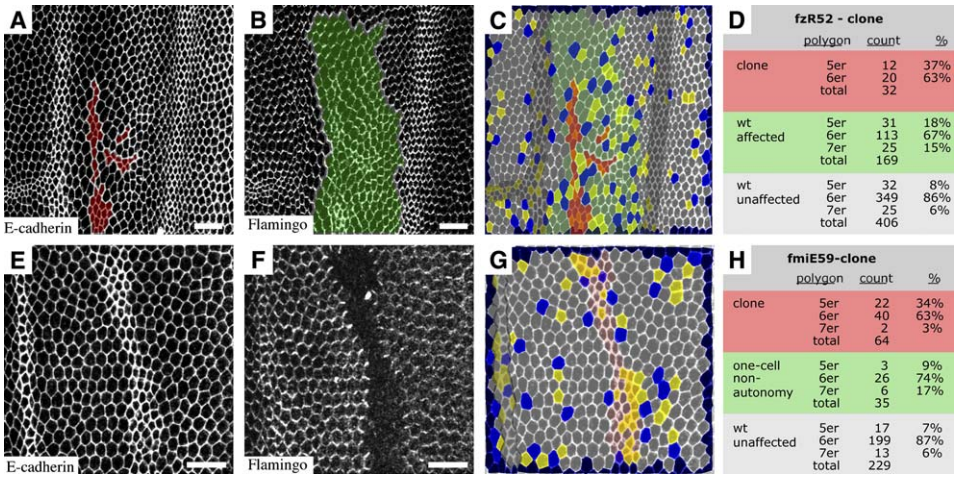

Figure 5. Cell Packing is Nonautonomously Perturbed by fz^{R52} Mutant Clones

All scale bars are 10 μm. Color coding for different sided polygons is as in Figure 1.

(A and B) A fz^{R52} clone (colored red in [A] and [C]) stained for (A) E-Cadherin and (B) Fmi. Cells with altered Fmi polarity are colored green. Cadherin levels are normally elevated in the anterior compartment in pupal wings, accounting for brighter staining in the right half of the image.

(C) Image shown in (A) color-coded for polygon identity and overlaid with colors indicating clone (red), nonautonomously mispolarized cells (green), and vein cells (dark gray).

(D) Different polygon classes in fz^{R52} mutant cells (red), wild-type cells with altered Fmi polarity (green), and unaffected wild-type cells (gray) from images shown in (A)–(C).

(E–G) A fmi^{E59} clone stained for (E) Cadherin and (F) Fmi and analyzed for (G) neighbor number. The clone is shaded pink. fmi^{E59} mutant cells are smaller than wild-type and have elevated E-Cadherin at apical junctions. The row of small cells to the left is a vein.

(H) Different polygon classes in fmi^{E59} mutant cells (red), wild-type cells directly adjacent to clone (green), and more distant wild-type cells (gray) derived from images shown in (E)–(G).

occur efficiently in the absence of products of the Pk-Sple locus.

Packing defects of the hypomorphic *Flamingo* (*fmi*) allele, $fmi(stan)^3$, are mild but significant (Figures 4C, 4E, 4F, and 4G and Table S2). The null allele fmi^{E59} produces much stronger defects (Table S2 and Figure 5). The variability of individual junctional lengths in these cells is more than twice that of wild-type, and only 69% of fmi^{E59} mutant cells become hexagonal, compared with 78% in wild-type (Table S2). Pentagonal cells persisted in fmi^{E59} mutants (27% compared with 13% in wild-type). This suggests that the majority of pentagonal cells fail to assemble boundaries with new neighbors when Fmi is missing.

We examined the packing geometry of two different *frizzled* (*fz*) alleles, fz^{R52} and fz^{P21}. fz^{P21} mutant wings fall into two classes. While the majority of wild-type and PCP mutant wings initiate hair formation by 42 hr after puparium formation (APF) (at 22ºC), a subset of fz^{P21} mutant wings does not. Since these wings were not apoptotic (as indicated by Caspase staining, data not shown), we included them in our analysis and quantified them separately. Even at 50 hr APF, their packing is much more irregular than that of wild-type (Figures 4C and 4E–4G and Table S2). Defects in fz^{P21} mutant wings that do initiate hair formation by 42 hr APF are milder but still significant (Figures 4C and 4E–4G and Table S2). fz^{R52} homozygotes do not produce viable pupae in our hands, and homozygous mutant clones are small. These clones have even stronger packing defects than those of fz^{P21}; cells in the clone shown in Figure 5 are 37% pentagonal, suggesting that little repacking occurs in fz^{R52} homozygous tissue. Thus, Fz is needed to develop regular hexagonal packing.

$stbm^6$ and dgo^{380} mutant wings have milder, but significant, alterations in the ratio of pentagons, hexagons, and heptagons (Figures 4C, 4E, and 4F and Table S2) and of four-way vertices (Figure S2G). Both mutants, however, affect junction length variability more strongly than $pk\text{-}sple^{13/26}$ (Figure 4G and Table S2). Taken together, these data indicate that PCP mutant cells fail to efficiently assemble boundaries with new neighbors and cannot regularize their packing geometry.

Fz Mutant Cells Alter the Packing of Adjacent Tissue

To ask whether interfering with PCP polarity could alter the geometry of packing in wild-type cells, we examined cells surrounding PCP mutant clones with either autonomous (fmi^{E59}) or nonautonomous (fz^{R52}) effects on polarity. We examined the frequency of pentagons, hexagons, and heptagons in fz^{R52} and fmi^{E59} mutant clones, and in the areas of disturbed and normal Fmi polarity surrounding both. The mutant cells within both fz^{R52} and fmi^{E59} clones are abnormally packed (Figures 5C, 5D, 5G, and 5H). However, whereas the packing defects caused by *Fmi* clones are predominantly restricted to the clone and directly adjacent cells (Figures 5E–5H), *Fz* clones alter packing over long distances in wild-type tissue (Figures 5A–5D) in the same regions where *Fmi* polarity is disturbed. The abnormal packing of wild-type cells surrounding fz^{R52} clones is unlikely to be a consequence of altered cell packing within the mutant clone, because fmi^{E59} mutant clones pack just as abnormally, but do not perturb packing in the surrounding tissue. This suggests that dominant reorientation of Fmi polarity by *frizzled* mutant clones disturbs the repacking of wild-type cells.

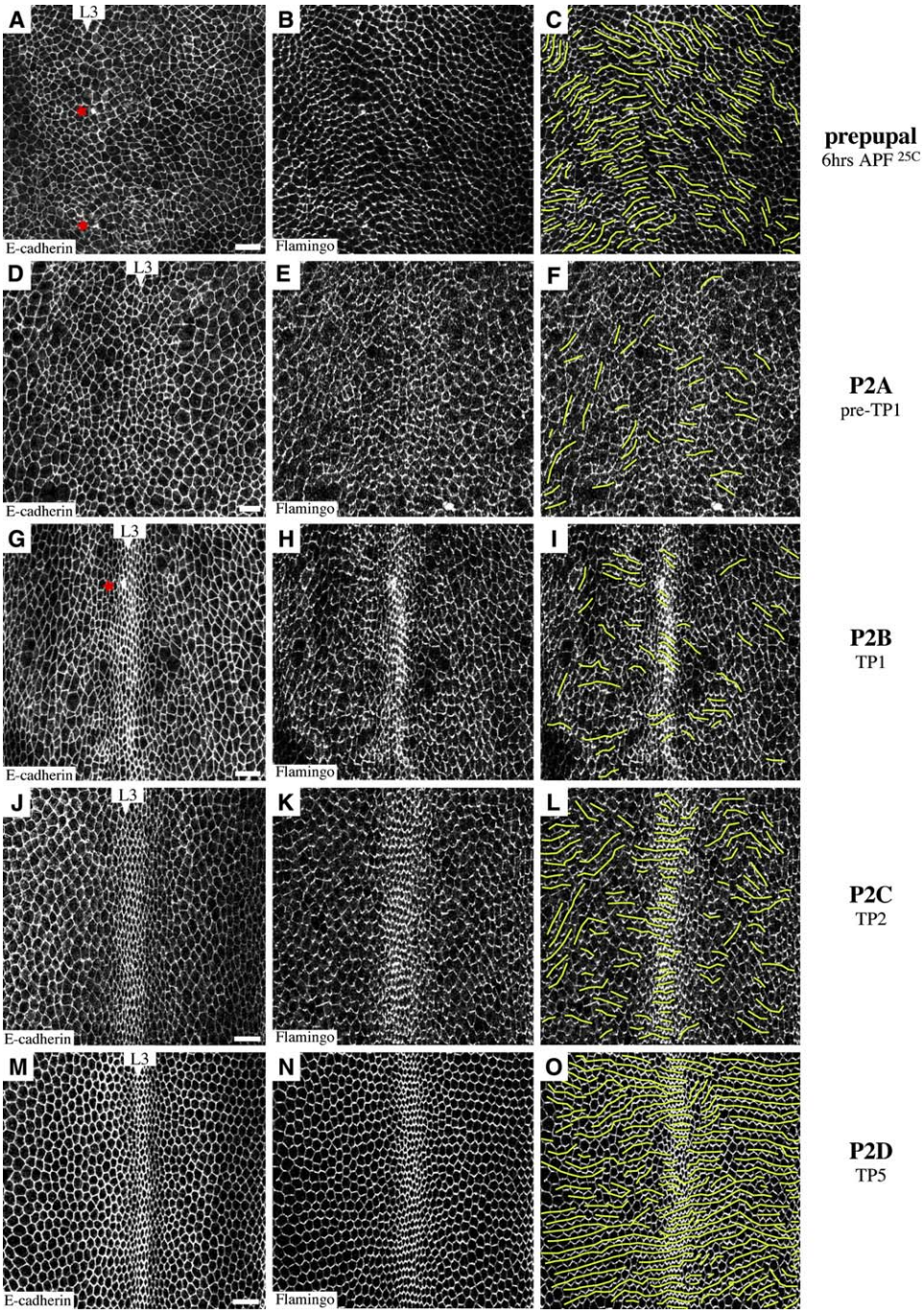

Figure 6. Fmi Polarity Is Perturbed during Junction Remodeling

(A–O) Fmi and Cadherin staining in the region surrounding L3 (arrowhead) at different developmental stages. Distal is up. Asterisks indicate the developing campaniform sensillum on L3. Green lines in (C), (F), (I), (L), and (O) are drawn between neighboring cells with coherent Fmi polarity, through boundaries with lower Fmi levels. All scale bars are 10 μm. (A–C) A prepupal wing imaged for (A) E-Cadherin:GFP and (B and C) Fmi. (D–F) Early pupal wing (Waddington P2A) stained for (D) E-Cadherin and (E and F) Fmi. (G–I) A pupal wing (Waddington P2B, TP1) stained for (G) E-cadherin and (H and I) Fmi. (J–L) A pupal wing at early P2C (TP2) stained for (J) E-Cadherin and (K and L) Fmi. (M–O) A pupal wing at Waddington stage P2D (TP5) stained for (M) E-Cadherin and (N and O) Fmi.

Fmi Polarity Is Transiently Disturbed during Junction Remodeling

To investigate how the PCP proteins were localized during repacking, we imaged pupal wings for Fmi before, during, and after hexagonal packing. Since it is thought that PCP proteins do not polarize until shortly before hair formation, we were surprised to find that the subcellular distribution of Fmi is polarized in many areas of the wing before junction remodeling is initiated, even in late third instar wing discs and prepupal wings (Figures S4A–S4D and Figures 6A–6C). Fz-GFP (Strutt, 2001) is distributed similarly (not shown). This polarity may have been

missed because it exhibits less long-range coherence in imaginal discs and prepupal wings than it does later.

In prepupal wings, Fmi polarity is roughly proximal-distal in the region surrounding L3 (Figures 6A–6C). Coherent Fmi polarity is lost at the beginning of the pupal period (Figures 6D–6F): this is exactly the time at which junction remodeling initiates. Although polarity is not coherent, Fmi is not uniformly distributed along cell boundaries. This can be clearly seen when Fmi localization (Figure 6E) is compared to that of E-Cadherin (Figure 6D).

At TP1, Fmi polarization begins in vein cells as they contract their apical cross-section (Figures 6G–6I). Intervein regions contain only small groups of cells with coherent polarity, and the axes of these groups are not always proximal-distal (Figures 6G–6I). By TP2, Fmi polarity is coherent between larger groups of cells, although the axis of polarity is still mixed (Figures 6J–6L). Fmi polarity is aligned in large coherent domains along the proximal-distal axis by TP4, when hexagonal packing is completed, and it remains unchanged at TP5 when hairs emerge (Figures 6M–6O). In summary, PCP proteins polarize during larval and prepupal stages, alignment of polarity between cells is disturbed when junction remodeling begins, and long-range polarity is reestablished as hexagonal packing is completed. Early polarization of PCP proteins is consistent with the genetic requirement for *fz* and *ds* activity at this time to determine the axis of polarity (Matakatsu and Blair, 2004; Strutt and Strutt, 2002a), and it suggests that the feedback loop that organizes coupled proximal and distal domains (Amonlirdviman et al., 2005; Tree et al., 2002b) probably acts during these early stages.

PCP Mutants Enhance Epithelial Disintegration Caused by a Lack of *dynamin*

We wondered whether PCP proteins might affect packing by influencing recycling of junctional components. Therefore, we asked whether PCP mutants enhanced the hole formation caused by *shi* loss of function. We shifted double mutant pupae to a subrestrictive temperature that never causes holes to form in *shi* mutants (Figure 7A) or in PCP mutants (not shown and Figure S5). When *shi* is combined with dgo^{380}, $stbm^{6}$, $stbm^{153}$, $stbm^{D}$, $stan^{3}$, $pk\text{-}spl^{1}$, or pk^{1}, hole formation occurs even under these mild conditions (Figure 7A). This raises the possibility that PCP proteins may worsen Cadherin recycling defects in *dynamin* mutant cells. Consistent with this, gaps in Cadherin arise more frequently in double $shi;pk^{1}$ or $shi;dgo^{380}$ mutant wings than in wings mutant for *shi* alone (Figures 7B–7D). This suggests that Cadherin is recycled less efficiently in the absence of PCP proteins.

Despite this enhancement, no striking abnormalities in Cadherin distribution were seen in most PCP mutants (Figure S5 and not shown). fz^{P21} mutant cells sometimes show gaps in E-Cadherin that are similar to, but much less frequent than, those of *shi* mutants (Figure 7G). In fmi^{E59} mutant cells, E-Cadherin levels are elevated (Figures 7E and 7F), but no gaps in localization are observed. These observations suggest that PCP proteins are not required for delivery of Cadherin to cell contacts during remodeling. Nevertheless, the PCP mutants enhance Cadherin recycling defects caused by loss of Dynamin. One model consistent with this shows that PCP proteins bias Cadherin recycling to specific places on the cortex. Reducing both the rate of recycling and its elevation at a particular site could exacerbate the failure of Cadherin delivery to growing cell boundaries.

Fmi Recruits the Exocyst Component Sec5

To test whether exocyst components were polarized by PCP proteins, we examined Sec5 localization during repacking of the wing epithelium. At this time, cell shapes are irregular, and Fmi polarity is not coherent between cells. Nevertheless, Fmi accumulates preferentially on specific regions of the cortex (Figure 8D). Although Sec5 vesicles are seen throughout the cell, they are particularly enriched near Fmi-positive cell boundaries (Figure 8C). Enrichment persists as Fmi polarity becomes aligned (Figures 8I–8K).

To test whether Fmi played an active role in recruiting Sec5, we overexpressed Fmi and examined Sec5 localization. Overexpressed Fmi is present uniformly around the cortex and in large punctate structures within the cell (Figures 8E and 8H). Sec5 dramatically accumulates in cells overexpressing Fmi and is recruited to sites of Fmi localization (Figures 8E, 8G, and 8H). Large internal structures positive for Fmi and Sec5 also contain Cadherin. (Figures 8E and 8F). These observations indicate that Fmi can recruit Sec5-positive vesicles containing E-Cadherin, and they suggest that PCP proteins may promote hexagonal packing by polarizing membrane trafficking.

Discussion

We have investigated the cellular mechanisms underlying hexagonal packing geometry in the wing epithelium. We find that the wing epithelium is irregularly packed throughout larval and prepupal development. Shortly before hair formation, it changes to a quasihexagonal array, suggesting that forces that promote surface area minimization may influence packing geometry as they appear to do in the retina (Hayashi and Carthew, 2004). Epithelial repacking occurs by growth and shrinkage of individual cell contacts that sometimes result in local neighbor exchanges after formation of a four-way vertex. Although the process superficially resembles changes in bubble packing in two-dimensional foams, epithelial cells, unlike bubbles, must build multiprotein complexes between new contacts and also disassemble them in a controlled fashion. Consistent with this, we find that recycling of junctional components, including Cadherin, is elevated during the process, and that recycling itself is required to support hexagonal packing.

What mechanisms might support assembly or disassembly of specific cell contacts? During embryonic gastrulation, shrinkage of individual cell contacts depends on the localized activity of myosin (Bertet et al., 2004). Interestingly, cortical actin-myosin-driven contractility is also required for the endocytosis of Cadherin in cultured epithelial cells (Sahai and Marshall, 2002), suggesting that the two mechanisms may be coordinated. Our data raise the possibility that polarized trafficking of Cadherin or other junction proteins may also play a role. PCP proteins are required to develop hexagonal packing and are nonuniformly distributed at junctions during remodeling. Interestingly, Sec5-positive vesicles

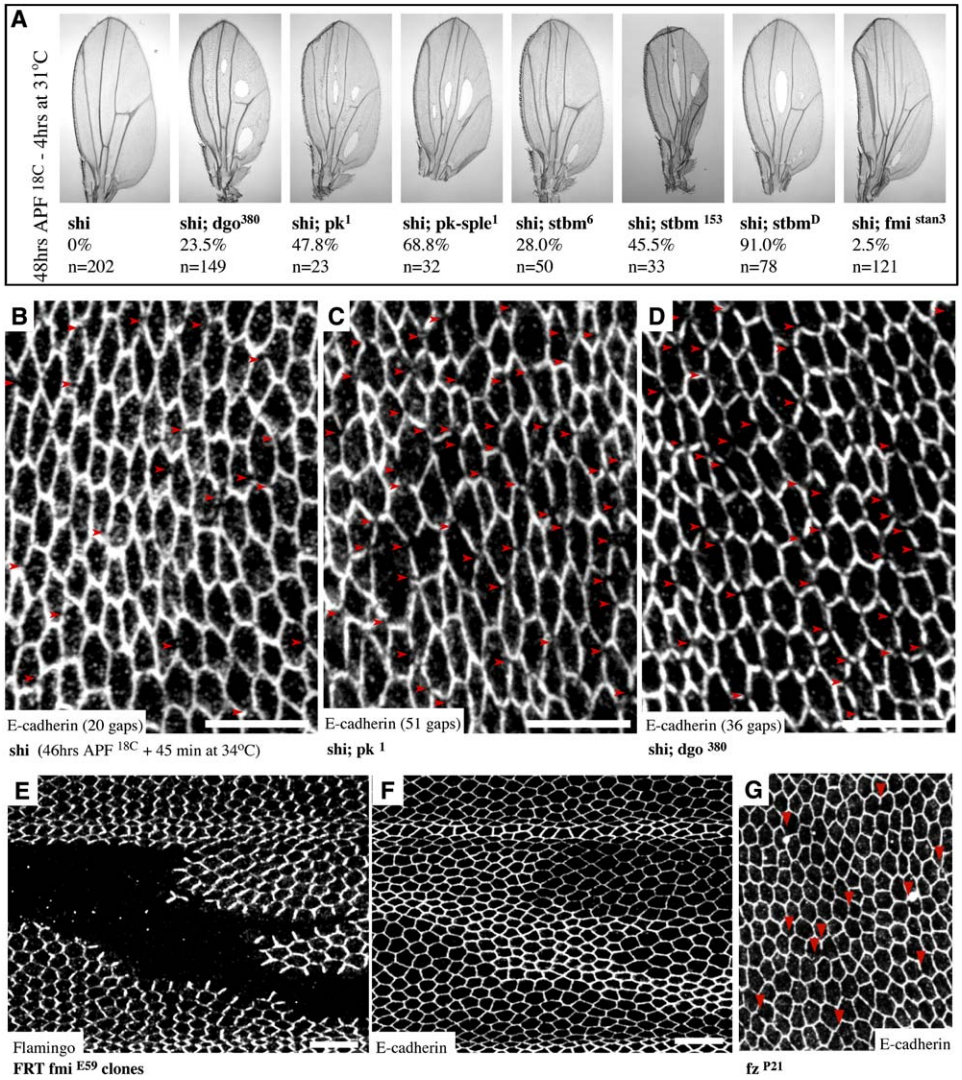

Figure 7. PCP Mutations Worsen Cadherin Recycling Defects

(A) Wings of the indicated genotypes were shifted to 31°C for 4 hr beginning at stage P2B. The percentage of wings forming holes is shown. n indicates the number of wings analyzed.

(B–D) Wings were temperature shifted, stained for E-Cadherin, and imaged in parallel under identical conditions. Arrows indicate gaps in junctional E-Cadherin. (B) *shi* mutant shifted to 34°C for 45 min during P2B. (C) *shi;pk*^{1} mutant wing shifted under the same conditions. (D) *shi;dgo*^{380} mutant wing shifted under the same conditions.

(E and F) a wing containing a *fmi*^{E59} mutant clone (indicated by loss of Fmi staining in [E], stained for [F] E-Cadherin).

(G) E-Cadherin-stained *fz*^{P21}/*fz*^{P21} wing. Red arrows indicate gaps in junctional E-Cadherin.

All scale bars are 10 μm.

concentrate near cortical regions rich in the PCP protein Fmi at this time, and Fmi overexpression recruits Sec5. Sec5 is part of a multiprotein complex called the exocyst that mediates polarized membrane delivery in a wide variety of contexts (Lipschutz and Mostov, 2002). In the thorax, the exocyst promotes delivery of E-Cadherin from recycling endosomes to the zonula adherens (Langevin et al., 2005). An intriguing possibility is that PCP proteins specify delivery to specific subregions of the zonula adherens where they are enriched. We cannot rule out the alternative possibility that PCP proteins regulate endocytosis of junctional components, however. In the oocyte, Sec5 has been found to associate very early with Clathrin-coated pits and Yolkless-containing endosomes destined for recycling (Sommer et al., 2005); therefore, accumulation of Sec5 need not reflect delivery to the plasma membrane.

We have not yet determined whether Sec5 is recruited to one or both sides of PCP boundaries, and the mechanism by which PCP proteins recruit Sec5 vesicles remains to be addressed. One possibility is that recruitment is mediated by activating Rho, a downstream effector of the PCP pathway (Winter et al., 2001); in yeast, Rho1 and Rho3 interact directly with components of the exocyst and affect polarized delivery of vesicles to the bud and docking at the plasma membrane. Alternatively, PCP proteins might recruit Sec5 simply by polarizing the actin cytoskeleton; exocyst vesicles travel to the yeast bud tip on polarized actin cables by using myosin motors (Pruyne et al., 1998), and we have noticed

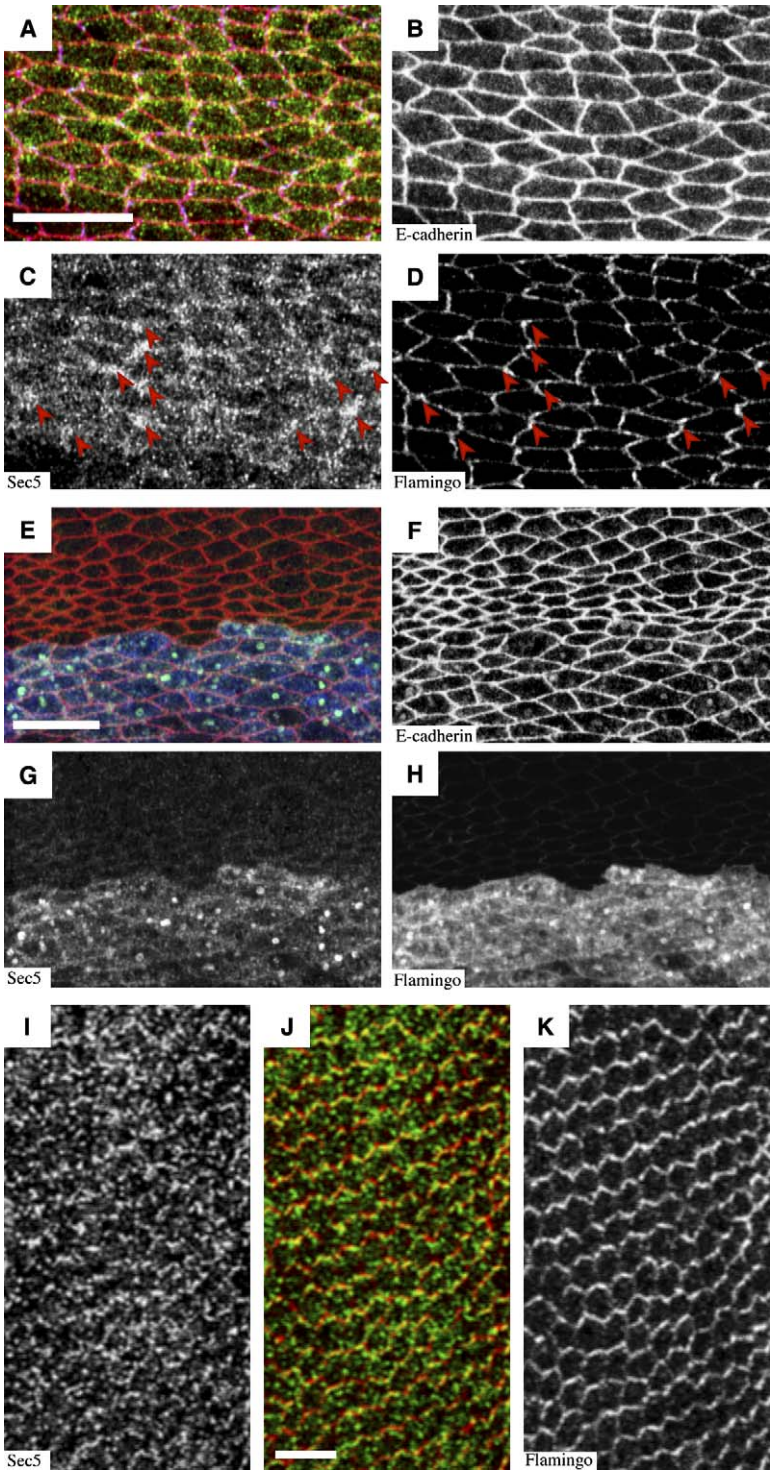

Figure 8. Sec5 Is Recruited by Fmi

(A–D) A wing undergoing repacking stained for (A and B) E-Cadherin (red), (A and C) Sec5 (green), and (A and D) Fmi (blue). Arrowheads indicate Sec5 accumulation near Fmi-enriched boundaries.

(E–H) A wing undergoing repacking and overexpressing (E and H) Fmi (blue) at the AP boundary. Acquisition settings were adjusted so that overexpressed Fmi was in the linear range, making endogenous Fmi undetectable. (E and G) Sec5 (green) accumulates with Fmi at the cortex and on vesicles that also contain (E and F) Cadherin (red).

(I–K) A hexagonally packed wing epithelium stained for (I and J) Sec5 (green) and (J and K) Fmi (red).

All scale bars are 10 μm.

that the nonmuscle Myosin Zipper accumulates near PCP domains (A-R.C., unpublished data). Physical interactions between PCP and exocyst components should also be investigated.

Do defects in packing geometry directly perturb hair polarity in PCP mutant wings? Our data do not support this idea; we searched assiduously, but without success, for correlations between regions of irregular packing and hair polarity defects. PCP proteins appear to regulate hexagonal packing and hair polarization independently. In this context, it would be interesting to investigate the role of polarized exocyst-mediated delivery in hair outgrowth.

The conserved cassette of PCP proteins controls a variety of seemingly different developmental processes, and no common cell biological mechanism has ever been proposed for their action (Copp et al., 2003; Maurus and Kuhl, 2004; McNeill, 2002; Mlodzik, 2002; Strutt,

2003; Veeman et al., 2003). Polarizing membrane trafficking by recruiting Sec5 is a basic function that could be utilized in many different contexts, and it may help explain the requirement of PCP proteins in a divergent set of processes. Both rotation of photoreceptor clusters (McNeill, 2002; Strutt and Strutt, 2002b) and convergent extension movements (Copp et al., 2003; Maurus and Kuhl, 2004) depend on the ability of cells to make and break intercellular contacts, as they do during hexagonal packing in the wing. Consistent with this, Silberblick (Wnt-11) acts through the PCP pathway and appears to affect endocytic trafficking of Cadherin during zebrafish gastrulation (Ulrich et al., 2005). Recruitment of exocyst components might also be a plausible mechanism to explain the ability of PCP proteins to bias Notch Delta signaling between R3 and R4 photoreceptors, since Delta delivery is dependent on the exocyst (Jafar-Nejad et al., 2005). In the future, identifying the chain of events that leads from PCP protein localization to exocyst recruitment may increase our understanding of these important processes.

Experimental Procedures

Immunofluorescence Microscopy

Pupal wings were dissected in fixative (8% [w/v] PFA, 200 mM sodium cacodylate, 100 mM sucrose, 40 mM potassium acetate, 10 mM sodium acetate, 10 mM EGTA) and washed in SPT (0.02% [w/v] saponin + 0.02% [w/v] Triton X-100/PBS). Wings were permeabilized for 30 min in PBT (0.1% [w/v] Triton X-100/PBS), washed in SPT, and then blocked for 30 min in SPN (SPT + 5% [w/v] normal goat serum). Primary antibodies/SPN (mouse anti-Fmi [1:20] [Usui et al., 1999] and rat anti-DE-cadherin [1:100] [Oda et al., 1994], rabbit anti-Sec5 [1:1000] [Sommer et al., 2005], and guinea pig anti-Coracle [1:3000] [Fehon et al., 1994]) were incubated at 4ºC overnight, washed in SPT, blocked in SPN, and incubated with secondary antibodies in SPN for 3 hr at room temperature, then mounted (ProLong Antifade, Molecular Probes) and imaged on a Zeiss Confocal Microscope.

Automated Image Analysis

Cell neighborhood analysis was performed by using Cellenger software (Definiens AG, Munich) and will be described elsewhere. Briefly, Cellenger uses a hierarchical classification to selectively combine small groups of pixels into larger objects such as cells, borders, and junctions. First, the algorithm classified "seed" regions in the center of each cell, which are defined as local regions of the lowest intensity. Seeds were expanded by iteratively adding pixels, which bordered the seed, by first adding darker and then lighter pixels. Simultaneous growth of all seeds in this manner resulted in good general convergence of seed perimeters with cell boundaries, which were finally optimized by edge smoothing. In their fully grown state, the seeds were classified as cells. All images were closely checked visually for mistakes in boundary recognition. If image contrast was poor, manual clean up of cell boundaries was required.

The algorithm then quantified neighbor number by the counting cells in direct contact with each cell in the image. A boundary had to be at least four pixels long to be considered as the side of a cell. If less than four pixels, the boundary was classified as a 4-fold vertex. Cells, which were only partly contained at the edge of the image, were completely excluded from analysis. Members of the outermost perimeter of cells completely contained within the image were classified as "edge" cells. Edge cells were counted as the neighbors of other cells, but the number of neighbors for edge cells was not counted.

Cell borders and vertices were classified in the following manner. For each cell a perimeter two pixels deep was reclassified as a "border." The border pixels from all cells were combined into a single object having the appearance of a meshwork. Intersection points were identified by attempting to overlay the meshwork with a variety of branched patterns. Those places where a branching pattern could be completely fit within the border meshwork were reclassified as "vertices." Vertices were further classified as 3-fold or 4-fold vertices according to the number of cells they contacted. Border pixels between vertices retained the classification "border"; each border then represented the common boundary between two cells.

Statistical data about the number of neighbor classes, cell perimeter, cell area, and individual boundary length between two vertices was provided by the Cellenger algorithm. Raw data output was further processed and analyzed with Microsoft Excel software.

Supplemental Data

Supplemental Data including quantitation of cell packing defects in PCP mutants (Tables S1 and S2); quantitation of wild-type packing in other wing regions (Figure S1); controls for *shibire* temperature shift experiments (Figure S2); controls for Rab11SN experiments and colocalization of Cadherin GFP with Rab5CFP (Figure S3); polarized localization of Flamingo in imaginal discs and prepupal wings (Figure S4); and normal Cadherin distribution in *dgo* and *pk* mutant wings at 34ºC are available at http://www.developmentalcell.com/cgi/content/full/9/6/805/DC1/.

Acknowledgments

A.K.-C. was supported by SPP 1111 from the Deutsche Forschungsgemeinschaft. We thank Francois Graner and Benjamin Dollet for stimulating discussions of foam behavior. We thank Ingmar Riedel for statistical advice. We gratefully acknowledge the support of the Max Planck Institute of Molecular Cell Biology and Genetics Light Microscopy Facility. We thank Tadashi Uemura and Sean Munro for generously providing antibodies, and we gratefully acknowledge fly stocks received from David Strutt, Hiroki Oda, Ulrich Tepass, and Sean Munro. We are grateful to Joe Howard, Annette Schenck, Kai Simons, and Marino Zerial for critical comments on the manuscript.

Received: February 9, 2005
Revised: August 19, 2005
Accepted: October 24, 2005
Published: December 5, 2005

References

Adler, P.N. (2002). Planar signaling and morphogenesis in *Drosophila*. Dev. Cell *2*, 525–535.

Amonlirdviman, K., Khare, N.A., Tree, D.N., Chen, W., Axelrod, J., and Tomlin, C.J. (2005). Mathematical modeling of planar cell polarity to understand domineering non-autonomy. Science *307*, 423–426.

Bertet, C., Sulak, L., and Lecuit, T. (2004). Myosin-dependent junction remodelling controls planar cell intercalation and axis elongation. Nature *429*, 667–671.

Bryant, D.M., and Stow, J.L. (2004). The ins and outs of E-cadherin trafficking. Trends Cell Biol. *14*, 427–434.

Copp, A.J., Greene, N.D., and Murdoch, J.N. (2003). The genetic basis of mammalian neurulation. Nat. Rev. Genet. *4*, 784–793.

Dumstrei, K., Wang, F., Shy, D., Tepass, U., and Hartenstein, V. (2002). Interaction between EGFR signaling and DE-cadherin during nervous system morphogenesis. Development *129*, 3983–3994.

Eaton, S. (2003). Cell biology of planar polarity transmission in the *Drosophila* wing. Mech. Dev. *120*, 1257–1264.

Fehon, R., Dawson, I., and Artavnis-Tsakonas, S. (1994). A *Drosophla* homologue of membrane-skeleton protein 4.1 is associated with septate junctions and is encoded by the *coracle* gene. Development *120*, 545–557.

Gubb, D., and Garcia-Bellido, A. (1982). A genetic analysis of the determination of cuticular polarity during the development of *Drosophila melanogaster*. J. Embryol. Exp. Morphol. *68*, 37–57.

Gubb, D., Green, C., Huen, D., Coulson, D., Johnson, G., Tree, D., Collier, S., and Roote, J. (1999). The balance between isoforms of the prickle LIM domain protein is critical for planar polarity in *Drosophila* imaginal discs. Genes Dev. *13*, 2315–2327.

Hayashi, T., and Carthew, R.W. (2004). Surface mechanics mediate pattern formation in the developing retina. Nature *431*, 647–652.

Jafar-Nejad, H., Andrews, H., Acar, M., Bayat, V., Wirtz-Peitz, F., Mehta, S., Knoblich, J., and Bellen, H. (2005). Sec15, a component of the exocyst, promotes Notch signaling during asymmetric division of *Drosophila* sensory organ precursors. Dev. Cell 9, 351–363.

Langevin, J., Morgan, M., Rosse, C., Racine, V., Sibarita, J., Aresta, S., Murthy, M., Schwarz, T., Camonis, J., and Bellaiche, Y. (2005). *Drosophila* Exocyst components Sec5, Sec6, and Sec15 regulate DE-Cadherin trafficking from recycling endosomes to the plasma membrane. Dev. Cell *9*, 1–12.

Lipschutz, J.H., and Mostov, K.E. (2002). Exocytosis: the many masters of the exocyst. Curr. Biol. *12*, R212–R214.

Lock, J.G., and Stow, J.L. (2005). Rab11 in recycling endosomes regulates the sorting and basolateral transport of E-cadherin. Mol. Biol. Cell *16*, 1744–1755.

Marois, E., Mahmoud, A., and Eaton, S. (2005). The endocytic pathway and formation of the Wingless morphogen gradient. Development, in press.

Matakatsu, H., and Blair, S.S. (2004). Interactions between Fat and Dachsous and the regulation of planar cell polarity in the *Drosophila* wing. Development *131*, 3785–3794.

Maurus, D., and Kuhl, M. (2004). Getting an embryo into shape. Bioessays *26*, 1272–1275.

McKenzie, E., Krupin, A., and Kelley, M.W. (2004). Cellular growth and rearrangement during the development of the mammalian organ of Corti. Dev. Dyn. *229*, 802–812.

McNeill, H. (2002). Planar polarity: location, location, location. Curr. Biol. *12*, R449–R451.

Mlodzik, M. (2002). Planar cell polarization: do the same mechanisms regulate *Drosophila* tissue polarity and vertebrate gastrulation? Trends Genet. *18*, 564–571.

Nagafuchi, A., Ishihara, S., and Tsukita, S. (1994). The roles of catenins in the cadherin-mediated cell adhesion: functional analysis of E-cadherin-alpha catenin fusion molecules. J. Cell Biol. *127*, 235–245.

Nardi, J., and Magee-Adams, S. (1986). Formation of scale spacing patterns in a moth wing. Dev. Biol. *116*, 278–290.

Nilsson, D. (1989). Optics and evolution of the compound eye. In Facets of Vision, D.G. Stavenga, and R.C. Hardie, eds. (Berlin, Heidelberg: Springer-Verlag), pp. 30–73.

Oda, H., and Tsukita, S. (1999). Dynamic features of adherens junctions during *Drosophila* embryonic epithelial morphogenesis revealed by a Dα-catenin-GFP fusion protein. Dev. Genes Evol. *209*, 218–225.

Oda, H., and Tsukita, S. (2001). Real-time imaging of cell-cell adherens junctions reveals that *Drosophila* mesoderm invagination begins with two phases of apical constriction of cells. J. Cell Sci. *114*, 493–501.

Oda, H., Uemura, T., Harada, Y., Iwai, Y., and Takeichi, M. (1994). A *Drosophila* homolog of cadherin associated with armadillo and essential for embryonic cell-cell adhesion. Dev. Biol. *165*, 716–726.

Pelissier, A., Chauvin, J.P., and Lecuit, T. (2003). Trafficking through Rab11 endosomes is required for cellularization during *Drosophila* embryogenesis. Curr. Biol. *13*, 1848–1857.

Prigent, M., Dubois, T., Raposo, G., Derrien, V., Tenza, D., Rosse, C., Camonis, J., and Chavrier, P. (2003). ARF6 controls post-endocytic recycling through its downstream exocyst complex effector. J. Cell Biol. *163*, 1111–1121.

Pruyne, D.W., Schott, D.H., and Bretscher, A. (1998). Tropomyosin-containing actin cables direct the Myo2p-dependent polarized delivery of secretory vesicles in budding yeast. J. Cell Biol. *143*, 1931–1945.

Roberts, W.M., Howard, J., and Hudspeth, A.J. (1988). Hair cells: transduction, tuning, and transmission in the inner ear. Annu. Rev. Cell Biol. *4*, 63–92.

Sahai, E., and Marshall, C.J. (2002). ROCK and Dia have opposing effects on adherens junctions downstream of Rho. Nat. Cell Biol. *4*, 408–415.

Sever, S. (2002). Dynamin and endocytosis. Curr. Opin. Cell Biol. *14*, 463–467.

Sommer, B., Oprins, A., Rabouille, C., and Munro, S. (2005). The exocyst component Sec5 is present on endocytic vesicles in the oocyte of *Drosophila melanogaster*. J. Cell Biol. *169*, 953–963.

Strutt, D.I. (2001). Asymmetric localization of frizzled and the establishment of cell polarity in the *Drosophila* wing. Mol. Cell *7*, 367–375.

Strutt, D.I. (2002). The asymmetric subcellular localisation of components of the planar polarity pathway. Semin. Cell Dev. Biol. *13*, 225–231.

Strutt, D. (2003). Frizzled signaling and cell polarization in *Drosophila* and vertebrates. Development *130*, 4501–4513.

Strutt, H., and Strutt, D. (2002a). Nonautonomous planar polarity patterning in *Drosophila*: dishevelled-independent functions of frizzled. Dev. Cell *3*, 851–863.

Strutt, H., and Strutt, D. (2002b). Planar polarity: photoreceptors on a high fat diet. Curr. Biol. *12*, R384–R385.

Tardieu, A. (1988). Eye lens proteins and transparency: from light transmission theory to solution X-ray structural analysis. Annu. Rev. Biophys. Biophys. Chem. *17*, 47–70.

Tepass, U., and Hartenstein, V. (1994). The development of cellular junctions in the *Drosophila* embryo. Dev. Biol. *161*, 563–596.

Tilney, L., and Saunders, J.C. (1983). Actin filaments, stereocilia, and hair cells of the bird cochlea I. Length, number, width, and distribution of stereocilia of each hair cell are related to the position of the hair cell on the cochlea. J. Cell Biol. *96*, 807–821.

Tilney, L.G., Tilney, M.S., Saunders, J.S., and DeRosier, D.J. (1986). Actin filiaments, stereocilia, and hair cells of the bird cochlea III. The development and differentiation of hair cells and stereocilia. Dev. Biol. *116*, 100–118.

Tree, D.R., Ma, D., and Axelrod, J.D. (2002a). A three-tiered mechanism for regulation of planar cell polarity. Semin. Cell Dev. Biol. *13*, 217–224.

Tree, D.R., Shulman, J.M., Rousset, R., Scott, M.P., Gubb, D., and Axelrod, J.D. (2002b). Prickle mediates feedback amplification to generate asymmetric planar cell polarity signaling. Cell *109*, 371–381.

Ulrich, F., Krieg, M., Schotz, E.M., Link, V., Castanon, I., Schnabel, V., Taubenberger, A., Mueller, D., Puech, P.H., and Heisenberg, C.P. (2005). Wnt11 functions in gastrulation by controlling cell cohesion through Rab5c and E-Cadherin. Dev. Cell *9*, 555–564.

Usui, T., Shima, Y., Shimada, Y., Hirano, S., Burgess, R.W., Schwarz, T.L., Takeichi, M., and Uemura, T. (1999). Fmi, a seven-pass transmembrane cadherin, regulates planar cell polarity under the control of Frizzled. Cell *98*, 585–595.

van Dam, E.M., and Stoorvogel, W. (2002). Dynamin-dependent transferrin receptor recycling by endosome-derived clathrin-coated vesicles. Mol. Biol. Cell *13*, 169–182.

Veeman, M.T., Axelrod, J.D., and Moon, R.T. (2003). A second canon. Functions and mechanisms of β-catenin-independent Wnt signaling. Dev. Cell *5*, 367–377.

Waddington, C.H. (1941). The genetic control of wing development in *Drosophila*. J. Genet. *41*, 75–139.

Winter, C.G., Wang, B., Ballew, A., Royou, A., Karess, R., Axelrod, J.D., and Luo, L. (2001). *Drosophila* Rho-associated kinase (Drok) links Frizzled-mediated planar cell polarity signaling to the actin cytoskeleton. Cell *105*, 81–91.

Wootton, R. (1992). Functional morphology of insect wings. Annu. Rev. Entomol. *37*, 113–140.

Zallen, J.A., and Zallen, R. (2004). Cell-pattern disordering during convergent extension in *Drosophila*. J. Phys. Condens. Matter *16*, S5073–S5080.

Zerial, M., and McBride, H. (2001). Rab proteins as membrane organizers. Nat. Rev. Mol. Cell Biol. *2*, 107–117.

Zhang, X.M., Ellis, S., Sriratana, A., Mitchell, C.A., and Rowe, T. (2004). Sec15 is an effector for the Rab11 GTPase in mammalian cells. J. Biol. Chem. *279*, 43027–43034.